

PFC/JA-96-29

## H Mode Confinement in Alcator C-Mod

M. Greenwald, R.L. Boivin, F. Bombarda<sup>1</sup>, P. Bonoli, C. Fiore,  
D. Garnier, J. Goetz, S. Golovato, M. Graf, R. Granetz,  
S. Horne, A. Hubbard, I. Hutchinson, J. Irby, B. LaBombard,  
B. Lipschultz, E. Marmor, M. May<sup>2</sup>, G. McCracken, P. O'Shea,  
J. Rice, J. Schachter, J. Snipes, P. Stek, Y. Takase,  
J. Terry, Y. Wang, R. Watterson, B. Welch<sup>3</sup>, S. Wolfe

September 1996

<sup>1</sup>Associazione ENEA-Euratom per la Fusione, 00044 Frascati, Italy.

<sup>2</sup>The Johns Hopkins University, Baltimore, MD 21218.

<sup>3</sup>Institute for Plasma Research, U. Md, College Park, MD 20742.

Submitted to Nuclear Fusion.

This work was supported by the U. S. Department of Energy Contract No. DE-AC02-78ET51013. Reproduction, translation, publication, use and disposal, in whole or in part by or for the United States government is permitted.

# H Mode Confinement in Alcator C-Mod

M. Greenwald, R.L. Boivin, F. Bombarda<sup>#</sup>, P. Bonoli, C. Fiore, D. Garnier, J. Goetz, S. Golovato, M. Graf, R. Granetz, S. Horne, A. Hubbard, I. Hutchinson, J. Irby, B. LaBombard, B. Lipschultz, E. Marmor, M. May\*, G. McCracken, P. O'Shea, J. Rice, J. Schachter, J. Snipes, P. Stek, Y. Takase, J. Terry, Y. Wang, R. Watterson, B. Welch<sup>+</sup>, S. Wolfe, *MIT - Plasma Fusion Center, Cambridge, MA. 02139*

*\*The Johns Hopkins University, Baltimore Md. 21218*

*<sup>+</sup>Institute for Plasma Research, U. Md, College Park, Md. 20742*

*<sup>#</sup>Associazione Euratom-ENEA, Sulla Fusione, 00044 Frascati, Italy*

## Abstract

A series of experiments, examining the confinement properties of ICRF heated H-mode plasmas, has been carried out on the C-Mod tokamak. C-Mod is a compact tokamak which operates at high particle, power, and current densities at toroidal fields up to 8T. Under these conditions the plasma is essentially thermal with very little contribution to the stored energy from energetic ions (typically no more than 5%) and with  $T_i \sim T_e$ . Most of the data were taken with the machine in a single-null "closed" divertor configuration with the plasma facing components clad in molybdenum tiles. The data include those taken both before and after the first wall surfaces were coated with boron, with emphasis on the latter. H-modes obtained from plasmas run on boronized walls typically had lower impurity content and radiated power and attained higher stored energy than those run on bare molybdenum. Confinement enhancement, the energy confinement time normalized to L-mode scaling, for discharges with boronized walls, ranged from 1.6 to 2.4. The unique operating regime of the C-Mod device provided a means for extending the

tests of global scaling laws to parameter ranges not previously accessible. For example, the C-Mod ELMfree data was found to be 1.1-1.6 times the ITERH93 scaling and the ELMy data almost 2.0-2.8 times the ITERH92 ELMy scaling law, suggesting that the size scaling in both scalings may be too strong. While both ELMfree and ELMy discharges were produced, the ELM characteristics were not easily compared to observations on other devices. No large, low frequency ELMs were seen despite the very high edge pressure and temperature gradients that were attained. For all of our H-mode discharges, a clear linear relationship between the edge temperature pedestal and the temperature gradient in the core plasma was observed; the discharges with the "best" transport barriers also showing the greatest improvement in core confinement. A summary of the data described in this paper is now available in the ITER H-mode database.

## Introduction

C-Mod is a compact high-field tokamak with a highly closed divertor and with capabilities for strong plasma shaping[1]. Its major radius is 0.68 m, minor radius is 0.22 and the toroidal field,  $B_T$ , has been operated from 2.6 to 8.0 T. The plasma current,  $I_p$ , for these studies ranged from approximately 0.8 to 1.2 MA. Typical plasma elongations are in the range 1.6 - 1.75. The plasmas are somewhat "D" shaped, though at the present time, the divertor geometry holds the lower triangularity to values in the range 0.5-0.6. Upper triangularity is typically 0.3-0.4. The plasma line averaged density,  $n_e$ , ranged from 1.3 to  $4.3 \times 10^{20}/m^3$ , with the better H-modes all above  $2 \times 10^{20}$ . The auxiliary heating method is ICRF; employing hydrogen minority in deuterium plasmas at  $B_T = 5.3T$  as the principal scenario. For these experiments, up to 3.5 MW of RF power were available. Because of the large B/R ratio in C-Mod, ohmic heating is never negligible, contributing 0.5 - 1.5

MW depending on plasma temperature and purity. The first wall is composed of molybdenum tiles and is designed to take the very high power loadings which occur in this experiment; values for the parallel heat flux up to  $0.5 \text{ GW/m}^2$  have been measured[2]. The C-Mod divertor geometry, combined with the high densities, results in very effective baffling of neutrals. Divertor compression, the ratio of neutral pressure in the divertor chamber to the pressure in main plasma chamber, ranges from 100 to 300[3].

H-modes are easily obtained in C-Mod with ohmic and RF heating, over a wide range in L-mode target conditions including densities up to  $3 \times 10^{20}/\text{m}^3$  and fields up to 8T[4]. The power required for the L-H transition is consistent with  $P_{\text{TOT}}/S = .02-.04 \text{ nB}$ ; with  $P_{\text{TOT}}$  measured in MW,  $S$  in  $\text{m}^2$ ,  $n$  in  $10^{20}/\text{m}^3$  and  $B_T$  in T. The factors that cause the variation in required input power are not well understood, but seem to be related to impurity levels, wall conditioning, and neutral pressure. Initially, the H-modes were characterized by strong, high frequency ELMs or brief ELM-free periods with accumulating impurities and high ratios of  $f_{\text{RAD}} = P_{\text{RAD}}/P_{\text{TOT}}$ . These results, combined with those reported on other devices[5], led us to study the effect of boronizing the vacuum chamber [6]. In C-Mod, vessel conditioning is accomplished via electron cyclotron discharge cleaning, ECDC, in which 2.5 kW of microwave power at 2.45 GHz are applied as the toroidal field is slowly ramped from .06 to .14 T (measured at  $R = .67\text{m}$ ), sweeping the resonance over the vacuum wall. For boronization, the discharge cleaning gas was replaced with a 9:1 mixture of He and diborane ( $\text{B}_2\text{D}_6$ ). The boron coating was renewed about once a week. Following boronization, radiated power, which was primarily due to molybdenum, was lower and H-mode performance was dramatically improved. Unless explicitly stated, results in this paper refer to discharges produced following the boronization campaign.

## Measurements and Methodology

The set of diagnostics available for transport studies on C-Mod includes ECE and Thomson scattering for measuring  $T_e(r,t)$ ; a two-color interferometer (TCI), reflectometry, and Thomson scattering for determining  $n_e(r,t)$ ; an array of high resolution X-ray spectrometers for measuring  $T_i(r,t)$ ; neutron emission diagnostics for determining  $T_i(0,t)$ ; a visible bremsstrahlung array for measuring  $Z_{\text{EFF}}(r,t)$ ; a bolometer array for measuring radiated power profiles,  $P_{\text{RAD}}(r,t)$ ; various spectrometers for determining impurity content; and a full set of magnetic diagnostics for calculating the MHD equilibrium and related quantities. The plasma stored energy is calculated by integration of the density and temperature profiles ( $W_{\text{KIN}}$ ) and by analysis of the equilibrium with the EFIT code[7] ( $W_{\text{MHD}}$ ). These generally agree to within 20%. Most of this discrepancy can be understood as the result of errors in experimentally measured quantities; estimates of these errors are summarized in table I. A residual systematic difference between the magnetic and kinetic calculations remains. The larger part of this difference can be explained as kinetic energy stored in the minority ion tail, leaving a residual systematic difference of less than 5% of the total. When suitable background data are available for subtraction of stray field effects, we can also obtain the stored energy by analysis of the diamagnetic loop signals. These are in good agreement with  $W_{\text{MHD}}$ . Shots for confinement analysis were chosen to be in quasi-steady state with respect to stored energy, density, and magnetic equilibrium. Time slices used for comparison with scaling laws were chosen with  $f_{\text{RAD}} < 0.5$ ;  $dW/dt < 0.35 P_{\text{in}}$ ;  $dn_e/dt < 0.4 n_e/\tau_E$ ; and  $q_{95} > 3$ . (The selection criteria correspond to that of reference [8,9].)

For full profile and time-dependent analysis the TRANSP[10] code is used. This code uses measured plasma profiles as inputs then calculates the electron and

ion heat balance, particle balance, and magnetic diffusion with a fixed boundary equilibrium. For ICRF heated plasmas, the full wave SPRUCE[11] code linked to the Fokker-Planck solver FPPRF[12] is used to calculate the heating power to ions and electrons. SPRUCE assumes perfect wave power absorption, and thus overestimates absorbed power. From transient analysis of RF perturbations, we estimate the absorbed fraction to be 90% +/- 10% and this number is used for all global calculations. For our H-modes, which are at high densities, code results indicate that the energy in fast ions is less than 5%. The “thermal” nature of these plasmas is confirmed by observation of sawtooth reheat rates, which show very little contribution to plasma heating from fast ions immediately following the turn-off of ICRF power. For similar reasons, the electron and ion temperatures are not very different. The ion-electron equilibration time,  $\tau_{ei}$ , ranges from 2 msec near the plasma edge to 10 msec in the core. These values are much less than the energy confinement time.

### **H-modes in C-Mod - Observations**

Figure 1 shows traces from a typical ELMfree H-mode, obtained after a short dithering period which occurs as the ICRF power rises. This discharge had a plasma current of 1.0 MA, toroidal field of 5.3 T and an elongation of 1.65; the safety factor at the 95% flux surface,  $q_{95} = 3.7$  during the H phase. There is no appreciable auxiliary-heated L phase in this discharge as the ohmic input power, by itself, is very close to the threshold. In fact, L-H dithers can be seen during the ohmic phase at .58 and .62 seconds. Once the plasma enters H-mode, strong increases are seen in density, stored energy, and confinement time. While the plasma density continues to ramp up during the entire H phase, the confinement enhancement,  $H_{ITER89}$ [13], reaches 2.4 then drops gradually as the radiated power increases. Stored energy also dips slightly before the end of the RF pulse for the

same reason. By the end of the RF pulse,  $f_{\text{RAD}} \sim 0.75$ . The increase in radiated power is attributed to a dramatic increase in impurity confinement which will be discussed in a later section.  $\beta_{\text{N}}$  reaches 1.5, which, while finite, is below the expected  $\beta$  limit which is calculated to be in the range 2.0-3.0. Since the machine is running at high field, this  $\beta$  corresponds to very high pressures; central values of 0.5 MPa are regularly attained. The strong sawteeth seen on the electron temperature are common for all RF heating discharges, whether in L-mode or H-mode.

Under similar conditions, but at a slightly higher target density, ELMy H-modes are obtained (Figure 2a). After an initial drop, the  $\text{H}\alpha$  light increases and eventually exceeds the L-mode levels. Most of this light originates in a high-density, low-temperature “radiative-condensation” region[14] located above the divertor “nose” on the inner wall of the vacuum vessel. On top of this steady  $\text{H}\alpha$  light, numerous sharp spikes can be seen. These are signatures of ELMs, which come in clusters and are somewhat correlated with sawteeth. In this case, the plasma density rise is faster initially, but saturates and remains essentially constant during the rest of the H phase. Energy confinement is not quite as good as in the ELMfree discharge,  $H_{\text{ITER89}}$  reaching 2.0 and remaining at that level. Radiated power is lower for the ELMy discharge,  $f_{\text{RAD}} < 0.3$  for the entire H phase. As we will discuss later, the impurity confinement for these discharges, while substantially higher than for L-mode, is well below the levels of the ELMfree discharges. Figure 2b. shows an expanded view of several traces for the same shot. Details of the ELMs can be seen in the  $\text{H}\alpha$  and the edge electron temperature which is measured via electron cyclotron emission (ECE). Some admixture of density perturbation may be present in the ECE signal as the 2nd harmonic emission is near cut off at these densities. None the less, the perturbations are “edge localized” and associated with a smaller average temperature pedestal, reduced impurity accumulation, and slightly reduced energy confinement.

As seen on many other devices[15-17], the H-mode transition is accompanied by a strong increase in the edge temperature and density. Figure 3 shows temperature profiles, taken with an ECE grating polychromator, comparing L and H modes with similar line averaged density, plasma current, and input power. Data from outside the separatrix are available from fast scanning probe measurements[18]. The resolution for the ECE measurement is about 1 cm and the combined errors in measurement and separatrix position are about 0.3-0.5 cm, thus we cannot yet resolve the width of the transport barrier. Similar data is shown in figure 4, where density profiles from Thomson scattering and reflectometry are plotted before and after an L-H transition. The sharp edge gradients characteristic of the H-mode transport barrier are clear, but instrumental resolution and positional uncertainties again limit resolution to about 1 cm. The reflectometry measurements also reveal that the transition is accompanied by a sharp drop in edge density fluctuations (figure 5). The decrease in fluctuations is always fast, typically occurring in less than 100  $\mu$ secs. The combination of strong edge gradients in temperature and density leads of course to a similarly strong edge pressure gradient. Even though the toroidal field is large, the edge  $\beta$  gradient,  $\beta'$ , is substantial. The parameter  $\alpha = R\beta'$  reaches values of at least 0.4-0.5 and stability analysis shows many discharges with edge gradients at or above the ideal stability limit. Nevertheless, no type I (giant) ELMs are observed. Future work in this area will concentrate on improving the resolution of the edge profile measurements.

Profiles in the scrape-off layer (SOL) outside the separatrix are also altered during the H-mode[3]. These profiles can not be characterized by a simple scrape-off length in either L or H-modes. Rather, the gradients are principally a function of local temperature; steepest near the separatrix, where the temperatures are highest, and flatter as one moves out from the separatrix, where the temperature is low. Following the L-H transition, the density and pressure scale lengths, near



the separatrix, drop by about a factor of 2 to 2 mm and 1 mm respectively; the latter number being roughly equal to the local poloidal ion-gyro radius. Temperature gradients are not as strongly affected and the temperature at the separatrix is approximately the same for L and H-modes. The implication of these measurements is that the H-mode transport barrier extends some short distance into the SOL. A side effect of these very sharp density gradients, is the necessity of moving the plasma closer to the ICRF antenna, at the L-H transition, in order to maintain ICRF antenna loading. As shown in figure 6, this does not result in any degradation in confinement even with a gap between the separatrix and a nominal outer limiting surface of 2-3 mm. (The estimated error for determining the separatrix position is also about 2-3 mm.)

### **Confinement Results**

The improvement in energy confinement between L and H-mode discharges can be clearly seen in figure 7, where the plasma stored energy is plotted vs. input power. While there is more scatter in the H-mode data, ELMfree H-modes have on average 2.2 times the stored energy of the L-modes. The corresponding ratio for ELMy plasmas is about 2. Figure 8 shows the confinement enhancement plotted against the radiated power fraction. This plot includes time slices with high radiated power which are excluded from the confinement data base. Above  $f_{\text{RAD}} \sim 0.5$ , H-mode confinement degrades approaching the L-mode values as  $f_{\text{RAD}}$  approaches 1.0. Remarkably, the global L-mode confinement is unchanged over the range in  $f_{\text{RAD}}$  from 0.2 - 1.0, showing an essential difference between L and H-mode confinement. At the moderately high temperatures of these discharges, radiation is peaked in the edge region. While this has little effect on L-mode plasmas, which already have a cool edge, it is devastating to the H-modes, which require a much hotter boundary. This result may explain, in part, the improvement in perform-

ance seen in H-modes with boronized walls. Figure 9 compares traces from ELMy H-modes with similar plasma current, density, and RF power taken before and after the boronization. The dramatic difference in radiated power, edge temperature, and confinement enhancement are clear. Profiles of the radiated power for the two shots are shown in figure 10; indicating strong core radiation from molybdenum for the unboronized discharge. The effect on confinement can be seen in figure 11 where a comparison of the recent H-modes, obtained with boronized walls, and older data with bare molybdenum[4] is shown. The older data has systematically higher radiated power and lower confinement, however this does not seem to be the only difference between the two sets of data, as the unboronized shots lie below the boronized ones for corresponding values of  $f_{\text{RAD}}$ . High values of H were also obtained for unboronized ohmic H-modes (which are not shown in the figure).

### Global Scaling

So far we have discussed our H-modes in relation to L-modes and to L-mode scaling. The parameter range for our H-modes is not yet sufficient to reveal significant scaling trends in these data by itself, however some features are worth discussing. L-mode data on C-Mod are consistent with ITER89-P, but a regression on the data yields a scaling much more "Goldston-like" [19,20] in its parametric dependence,  $\tau_E \sim I_P/P^{1/2}$ , though with a coefficient about 50% larger than reference [20]. The new H-mode data are consistent with a multiplier of about 2 compared to our own L-mode scaling. Though we have no data below  $q_{95} \sim 3$  where confinement degradation has been reported[8], there is no clear dependence of the H-mode enhancement over a range in  $q_{95}$  from 3 to 5. This can be seen in figures 12a and 12b where the H factor (relative to H-mode scaling laws), is plotted vs.  $q_{95}$ . Here we are concerned only with the trend vs.  $q_{95}$ ; the discrepancies with the scaling laws

will be discussed in the next section. As seen on other machines[15], the best H modes have confinement times that approach but do not exceed values from ohmic, neo-Alcator scaling [21].

An obvious question is how C-Mod data compare to scaling laws previously derived from other machines. The ITER database group has assembled a large data set from a number of tokamaks and carried out systematic scaling studies[9]. Regressions are available for ELMfree and ELMy discharges and for total and thermal stored energy. We note at the outset that for C-Mod parameters, the thermal energy, calculated from these regressions, exceeds the total energy; an obvious impossibility. Figure 12a shows C-Mod ELMfree data compared with the corresponding ITERH93-P scaling law,  $\tau_E = 0.048 I_P^{0.87} B_T^{0.45} n_{eff}^{0.43} R^{1.84} n_e^{0.03} \epsilon^{-0.02} \kappa^{0.53} P_L^{-0.55}$ . Where the units are  $I_P$  in MA,  $B_T$  in T,  $R$  in meters,  $n_e$  in  $10^{20}/m^3$  and  $P_L = P_{TOT} - dW/dt$  in MW. In this case the  $H_H$  factor refers to enhancement above the nominal H-mode scaling so  $H_H = 1$  corresponds to a match between the data and the scaling law. The C-Mod data are systematically above the  $H_H=1$  line indicating better than predicted results. Figure 12b is a similar plot, for ELMy data where the ITERH92-P(ELMy) scaling predicts  $\tau_E = 0.068 I_P^{0.9} B_T^{0.05} n_{eff}^{0.4} R^{2.1} n_e^{0.3} \epsilon^{0.2} \kappa^{0.8} P_L^{-0.65}$  [22]. In this case the C-Mod data average about twice the predicted value. A possible culprit is the large size dependence seen in the scaling law. Also plotted on this figure is a comparison between the data and another commonly used expression to predict energy confinement for ELMy H-modes, namely 0.85 times the ELMfree expression. While this is an improvement over the ELMy law, it underestimates the C-Mod data by factors of 1.0-1.6. Another interesting exercise is to compare to the scaling derived from controlled experiments on JET and DIII-D[23], two machines with plasma shapes similar to C-Mod. In this case, a scaling for ELMfree H-modes, with dependences on  $P_L$ ,  $I_P$ , which are evident from the individual data sets and a scaling for R de-

terminated by comparison between the machines was reported. The authors also derived possible dependences on  $n$  and  $B$  from dimensional arguments. In this case, unique coefficients for  $n$  and  $B$  were not obtained, but instead, an equation relating the coefficient was derived consistent with the dimensionless, high- $b$  constraint. Two possible sets of coefficients were calculated in their paper, chosen to bracket dependences seen in other data. The results of a comparison between these results and C-Mod data are shown in figure 13. The standard JET-DIII-D scaling law,  $\tau_E = 0.106 I_P^{1.03} R^{1.48} P_L^{0.46}$ , underestimates the C-Mod results by a factor of 1.7. This is not necessarily surprising because C-Mod was not run at the same  $B_T$  and  $n_e$  as the JET and DIII-D data. Of the extended scaling laws, with  $n$  and  $B$  included; the first, with substantial  $B$  dependence fails to fit the C-Mod data by the same margin as the un-extended law. The second extension, with very weak  $n$  and  $B$  scaling but with less size dependence,  $\tau_E = 0.14 I_P^{1.06} R^{1.4} P_L^{-0.45} B_T^{0.06} n_e^{0.07}$ , is much closer to C-Mod. As with the ITER scaling laws, our data suggest that the size scaling of the nominal JET-DIII-D law may be too strong.

### Temperature Pedestal and Core Transport

The most salient feature of H-mode plasmas is the edge temperature pedestal, which on C-Mod can vary from 0.25 to 0.8 keV. Not surprisingly, the largest pedestals tend to occur in ELMfree discharges with low radiated power; the smallest pedestals are correlated with ELMy or radiative discharges. Quantitatively, there is a clear correlation between the quality of confinement in H-mode and the height of the edge pedestal. In figure 14,  $H_{ITER89}$  is plotted vs. the electron temperature measured at the 95% flux surface. There appears to be an offset linear relationship between the H factor and the edge temperature; a trend that also fits a small set of L-mode data which is shown as well. The L-mode data are chosen to have engineering parameters as close as possible to the H-modes. While the edge

pedestal, by itself, can account for a part of the stored energy increase seen in H-mode, a significant improvement in core confinement is observed as well[15]. Figure 15 shows profiles of thermal diffusivity comparing an H-mode discharge with an L-mode discharge with similar global parameters. At the densities present in these discharges, the measurements of the  $T_e$  and  $T_i$  profiles are not accurate enough to separate out the transport channels. Instead, we have plotted  $\chi_{\text{eff}}$  defined by  $\chi_{\text{eff}} \equiv (q_i + q_e) / (n_e \nabla T_e + n_i \nabla T_i)$ . What is found for these discharges and other similar pairs, is that the diffusivity in H-mode is about a factor of 2 lower than in L-mode plasma, across most of the profile. Measurements in the SOL also show  $\chi_{\text{perp}}$  dropping by about a factor of 2 over a distance of 2-3 mm from the separatrix[3]. This implies that the transport barrier extends a few ion poloidal gyro-radii into the scrape-off plasma.

Another interesting feature, seen in our data, is the relationship between the quality of the edge transport barrier and the improvement in core transport. Figure 3 shows temperature profiles from an L-mode discharge, an ELMy H-mode, and an ELMfree H-mode. Two trends are obvious: 1) the discharges with the highest temperature pedestals have the best global confinement (as previously discussed) and 2) the discharges with the best confinement also have the highest temperatures gradients in the plasma core. This point is made again in figure 16, where the core temperature gradient is plotted against the edge pedestal height. The data show an offset linear relationship between the edge temperature and the core temperature gradient. Such a simple relationship raises the question about the role of marginal stability or critical gradients in determining plasma transport.

## Impurity Transport

The increase in impurity levels that was discussed in an earlier section is not due to an increase in impurity source levels or to an improvement in impurity penetration. Impurity screening experiments indicate that the fractional penetration of injected gaseous impurities is lower in H-mode than in L-mode. Instead, the important factor in raising impurity levels is a dramatic increase in impurity confinement [24-26]. This phenomenon can be investigated by following the transport of trace amounts of non-intrinsic, non-recycling impurities which are injected into the plasma by the laser blow-off technique[27]. Figure 17 shows examples where scandium was injected into L and ELMy H mode plasmas. Brightness profiles of lines from He-like and Li-like Sc were measured with an array of high resolution X-ray spectrometers (HIREX[28]) and a scanning XUV grazing incidence spectrometer[29]. The He-like scandium exists in the plasma core, while the Li-like is peaked at  $r/a \sim 0.8$ . Two important features of these experiments are evident; the decay times for impurities,  $\tau_I$ , in the H-mode plasmas are much longer than in L-mode; and the amount of impurities which find their way to the plasma core is much greater. Impurity confinement times in ELMy H-mode are at least 0.2 seconds compared to  $\sim 0.02$  seconds in L-mode. This ratio is much larger than the corresponding ratio for energy confinement times; in H-mode,  $\tau_I$  is at least  $3 \times \tau_E$ . During ELMfree discharges the impurity confinement can be even longer, so long that an accurate measurement is not possible. We estimate that  $\tau_I > 0.5$  sec. for these cases.

Because spatial and temporal data are available from the measurements, it is possible to compare the measurements to transport simulations using the MIST code[30,31], where the transport is modeled as  $\Gamma = -D(r) \nabla n_I + V(r)n_I$ . While this approach does not necessarily produce a unique solution for the transport coeffi-

icients, it does demonstrate essential features which those coefficients must have. To account for the long decay time, the diffusion coefficient must be substantially lower in H-mode plasmas, while the increase in impurity inventory can be explained by a strong inward pinch, localized in the plasma edge. An example of transport coefficients which can produce a good match to the data is shown in figure 18. These results are similar to those reported on DIII-D[32] although those transport coefficients are substantially larger than the ones shown here for C-Mod. It is also worth noting the similarity in magnitude between the diffusion coefficients shown here and the thermal diffusivity shown in figure 15. The two sets of curves are of the same magnitude and the reduction in diffusivity seen at the L-H transition is about a factor of two in both cases. There is no analogy to the very strong inward pinch seen in the particle transport and this accounts for the very different values for particle and energy global confinement.

### **Summary and Discussion**

We have reported on energy and impurity particle confinement in ELMy and ELMfree H-modes in a high-field, high-density regime. The beneficial effects of boronization were demonstrated once again; plasmas run on boronized walls had better confinement and lower radiated power than those run on untreated molybdenum. It is important to note that the surface power densities in C-Mod exceeds that of all other tokamaks, reaching values predicted for ITER or other burning-plasma devices. With boronization, confinement enhancements over 2 were routinely obtained for a period of many confinement times. Quasi-steady conditions were reached in ELMy, enhanced-recycling discharges. Energy and particle diffusivities were found to be of the same magnitude and each decreases by approximately a factor of 2 after an L-H transition. The difference - the global impurity confinement being many times longer than energy confinement in H-mode - is at-

tributed to a strong inward particle pinch at the discharge periphery. We have found a clear linear relationship between the edge pedestal temperature and the core temperature gradient. This behavior is consistent with critical gradient models (for example ITG theories) but confirmation awaits quantitative comparisons.

In our studies of H-mode plasmas, we have measured energy confinement times that are consistently higher than what is predicted by the commonly used scaling laws. These scaling laws, which have a 10-20% root mean square error about the data that were used to derive them, did not reference C-Mod data; thus our experiments provide an excellent test for extrapolation of these laws. The result, that C-Mod data lie outside the fitting errors, should call into question the use of these laws for extrapolation. In particular, attention needs to be paid to scaling law dependences which are not readily apparent in data from individual machines. In this case, data covariances which naturally occur, may be corrupting the results. For example,  $\tau_E$  is usually seen to have only weak dependence on  $n$  or  $B$  [8,24], however  $n$ ,  $B$ , and  $R$  have a natural covariance through the density limit which scales roughly as  $B/R$  and could result in incorrect fitting coefficients for all three variables. In particular, our data may suggest that the size scaling in the scaling laws is too strong. Other variables, divertor compression and neutral pressure for example (which are very high in C-Mod), may be important for H-mode confinement, and are not yet included in empirical scaling laws. Of course, in the absence of a comprehensive first principles theory for plasma transport, empirical scaling will remain an essential tool, but we must constantly remind ourselves of the limitations of that approach.

## **Acknowledgements**

The authors wish to thank the rest of the Alcator team, the technical staff, engineers, students, and scientists whose hard work keeps the machine running



and productive. This work was supported by DOE contract No. DE-AC02-78ET51013

## References

- [1] I. HUTCHINSON, R. BOIVIN, F. BOMBARDA,, et al., *Phys. of Plasmas* **2**, **1** (1994), 1511
- [2] B. LIPSCHULTZ, B. LaBOMBARD, B. McCRACKEN, et al., "Modification of the Divertor Detachment Onset Density, in proceedings of the 12th International Conference on Plasma Surface Interactions in Controlled Fusion Devices, St. Raphael, France, 1996. To be published in *J. Nucl. Materials*
- [3] B. LaBOMBARD, J.L. GOETZ, I. HUTCHINSON, et al., "Experimental Investigation of Transport Phenomena in the Scrape-off Layer and Divertor", in proceedings of the 12th International Conference on Plasma Surface Interactions in Controlled Fusion Devices, St. Raphael, France, 1996. To be published in *J. Nucl. Materials*
- [4] J. A. SNIPES, R. L. BOIVIN, C. CHRISTENSEN, et al., *Physics of Plasmas*, **3** (1996) 1992.
- [5] U. SCHNEIDER., W. POSCHENRIEDER, M. BESSENRODT-WEBERPALS, et al., *J. Nucl Mater.* **176 &177** (1990), 311.  
G.L. JACKSON, J. WINTER, T.S. TAYLOR, et al., *Phys. Fluids B*, **4** (1992), 2181
- [6] J. WINTER, et al., *J. Nucl. Mater.*, **162-164** (1989), 713.
- [7] L. LAO, H. ST. JOHN, R. STAMBAUGH, A. KELLMAN, AND W. PFEIFFER, *Nucl. Fusion* **25**, (1985). 1611
- [8] J.P. CHRISTIENSEN, J.G. CORDEY, K. THOMSEN, et al., *Nucl. Fusion*, **32** (1992) 291
- [9] ITER H-MODE DATABASE WORKING GROUP, *Nucl. Fusion*, **34**, (1994), 131
- [10] HAWRYLUK, R., *Physics of Plasmas Close to Thermonuclear Conditions*, Proceedings of the course held in Varenna, Italy, **1**, **19** (1979)
- [11] D. SMITH, P. COLESTOCK, R. KASHUBA, T. KAMMASH, *Nucl. Fus.*, **27**, 1319 (1987)
- [12] G. HAMMET, "Fast Ion Studies of Ion Cyclotron Heating in the PLT Tokamak", PhD. thesis, Princeton University, 1986
- [13] P. YUSHMANOV, T. TAKIZUKA,, K. RIEDEL, O. KARDAUN, J. CORDEY, S. KAYE, D. POST, *Nucl. Fus.* **30**, (1990), 1999.
- [14] B. LIPSCHULTZ,, B. LaBOMBARD, E.S. MARMAR, et al., *Nucl. Fusion* **24** (1984) 977
- [15] F. WAGNER, G. Becker, K. Behringer, et al., *Phys. Rev. Lett.*, **49** (1982), 1408.
- [16] S.M. KAYE, M.G. BELL, K. BOL, et al., *J. Nucl. Mater.* **121**, (1984), 115.

- [17] G.L. JAHNS, R.J. GROEBNER, H. St. JOHN, Nucl Fusion **29**, (1989), 1271.  
ASDEX TEAM, Nucl. Fusion **29** (1989), 1959.
- [18] B. LaBOMBARD, J. GOETZ, C. KURZ, et al., Phys. Plasmas **2**, **6** (1995)  
2242
- [19] M. GREENWALD, R.L. BOIVIN, F. BOMBARDA, et al., Physics of Plasmas **2**, **6**  
(1995) 2305
- [20] R.J. GOLDSTON, Plasma Phys. and Cont. Fusion, **26**, (1984), 87.
- [21] R. R. PARKER, M. GREENWALD, S. C. LUCKHARDT, E. S. MARMAR, M.  
PORKOLAB, S. M. WOLFE, Nucl. Fusion **25** (1985) 1127.
- [22] ITER H-MODE DATABASE WORKING GROUP, Plasma Physics and Controlled  
Fusion (Proc. 14th Int. Conf. Wurzburg, 1992), Vol. 3, IAEA, Vienna  
(1993) 251.
- [23] D.P. SCHISSEL, J.C.DEBOO, K.H. BURRELL, et al., Nucl. Fusion, **31**  
(1991) 73
- [24] ASDEX TEAM, Nucl. Fusion **29** (1989), 1959.
- [25] K. IDA, R.J. FONCK, .S. SESNICK, R.A. HULSE, B. LeBLANC, S.F. PAUL,  
Nucl. Fusion **29** (1989), 231.
- [26] JET TEAM, Plasma Physics and Controlled Nuclear Fusion Research, 1990,  
(IAEA, Vienna, 1991), Vol. I, 261.
- [27] E.S. MARMAR, J.A. CECCHI, S.A. COHEN, Rev. Sci. Inst., **46** (1975, 1149.  
M. GRAF, "Impurity Injection Experiments on the Alcator C-Mod Tokamak",  
PhD. Thesis, Massachusetts Institute of Technology, 1995.
- [28] J.E.RICE AND E.S.MARMAR, Rev. Sci. Instrum. **{61}**, 2753 (1990)
- [29] J.L. TERRY, H.L. MANNING, E.S. MARMAR, Proc. of SPIE - The  
International Soc. for Optical Eng. Vol. 689 (1986) p. 54-60
- [30] R. A. HULSE, Nucl. Tech./Fusion, **3**, (1983), 259
- [31] YING WANG, "A Study of Impurity Screening in Alcator C-Mod Plasmas",  
PhD Thesis, Massachusets Institute of Technology, 1996
- [32] M.E. PERRY, N.H. BROOKS, D.A. CONTENT, R.A. HULSE, M. Ali MAH-  
DAVI, H.W. MOOS, Nucl. Fusion, **31** (1991) 1859.

**Table I.**

<b>Measured Quantity</b>	<b>Estimated Error</b>
$I_P$	3kA
$B_T$	0.03 T
$\beta_P$	0.05-0.1
$W_{MHD}$	10-15 kJ +5-10%
$n_e$	5-10%
$T_e$	10%
$T_i$	10-20%
$W_{KIN}$	20%
$P_{RAD}$	15-20%
$P_{icrf}$	10%

**Table Caption**

I. Estimated errors of various measured and calculated quantities.

## Figure Captions

1. Traces from an ELMfree H-mode discharge - shot number 960116024.
2. a. Traces from an ELMy H-mode - shot number 960116027. b. Same discharge as 2a. but with expanded time scale showing ELMs.
3. Temperature profiles from L and H modes (ELMy and ELMfree). The calculated separatrix positions for all three shot are the same, 0.896 m., Estimated error in the separatrix position is .002-.003 m.
4. Density profiles from L and H demonstrating edge pedestal.
5. Drop in edge fluctuations at L-H transition from reflectometry measurements at 88 GHz. Fluctuations drop in less than 100 micro seconds following the transition.
6. Energy confinement enhancement vs. outer gap. The estimated error for determining the separatrix position is 2-3 mm.
7. Stored energy vs. total input power ( $P_{TOT}$ ) for L and H modes
8.  $H_{ITER89}$  vs.  $P_{RAD}/P_{TOT}$  for L and H modes (H modes are for boronized discharges only)
- 9 Comparison of H-modes with boronized and unboronized walls. Note the dramatic difference in radiated power and confinement enhancement. The apparent increase in edge  $T_e$  seen after 1 second is an artifact of the toroidal field ramp down.
10. Radiated power profiles for the two shots shown in figure 9.
11.  $H_{ITER89}$  vs.  $P_{RAD}/P_{TOT}$  for boronized and unboronized H-modes.
12. a.  $H_{ITER94}$  vs. q95 for ELMfree data. b.  $H_{ITER92}$  vs. q95 for ELMy data.
13.  $H_{JET-D3D}$  for all three versions of scaling law.
14.  $H_{ITER89}$  vs. edge temperature pedestal,  $T_e(\psi=95)$ .
15.  $\chi_{eff}$  vs. r/a for L and H modes.
16. Grad  $T_e$  in core vs.  $T_e(\psi=95)$ .
17. Scandium radiation after laser blow-off for L and H modes.
18. Particle transport coefficients, D and V from impurity injection.

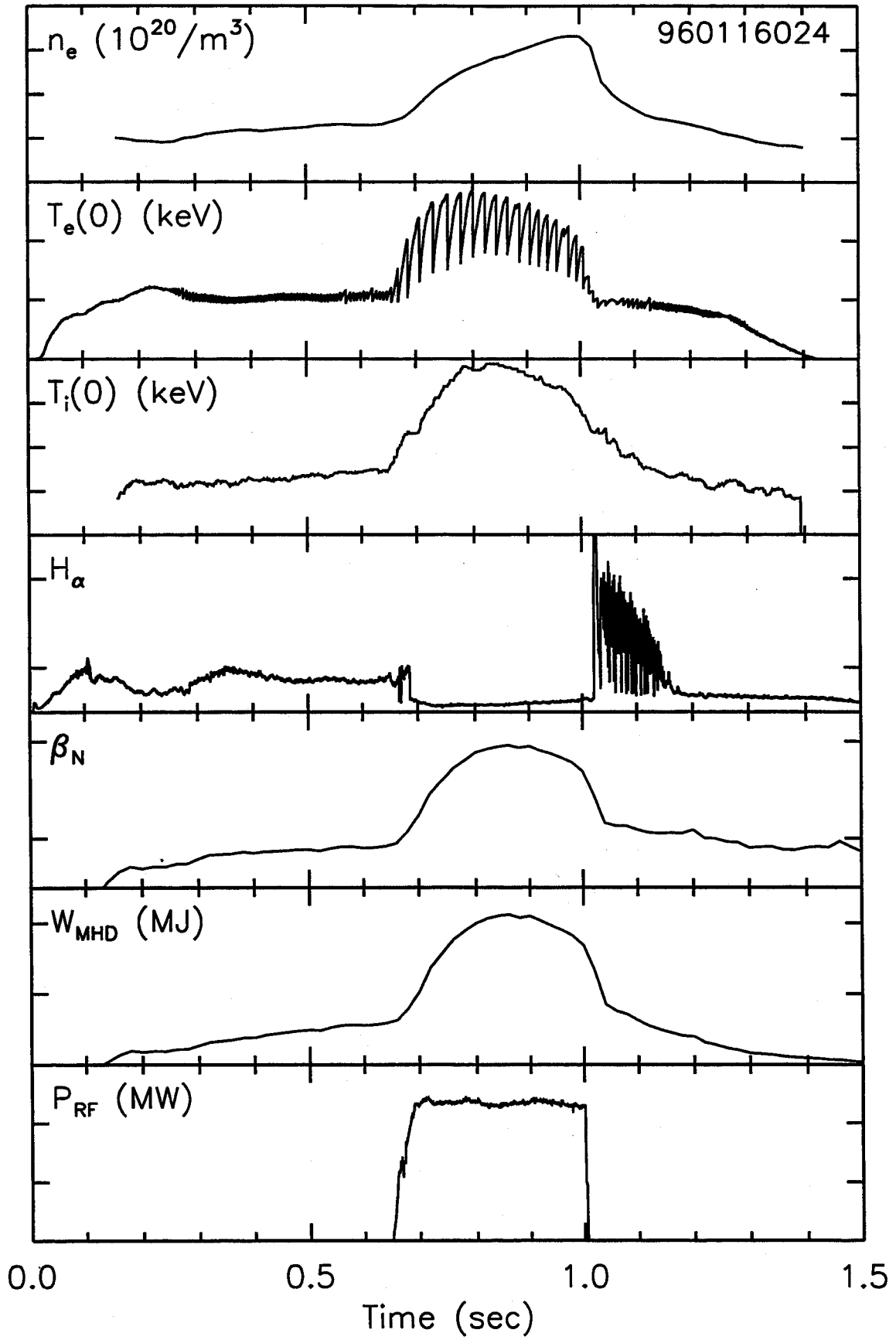


Figure 1

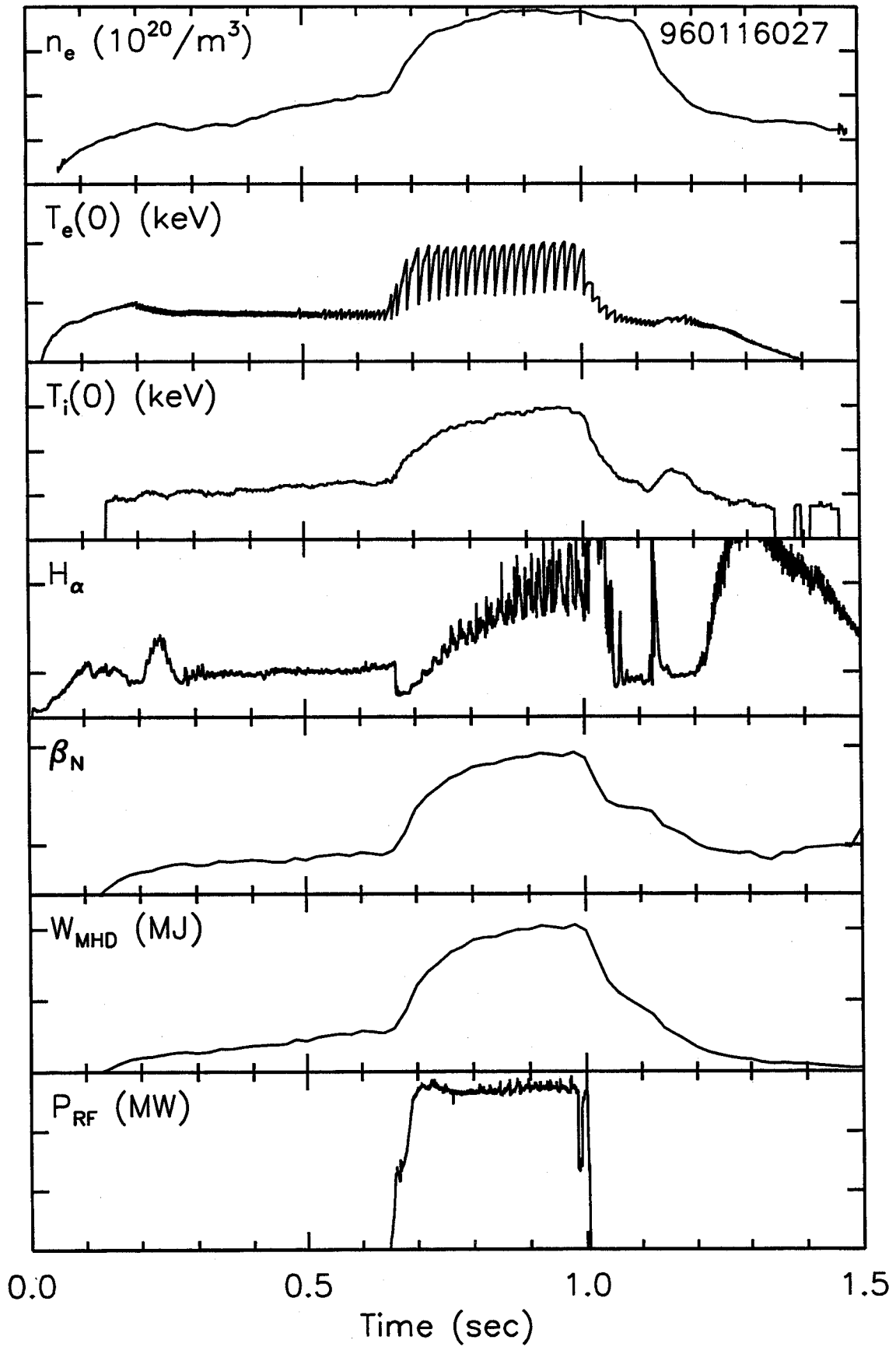


Figure 2(a)

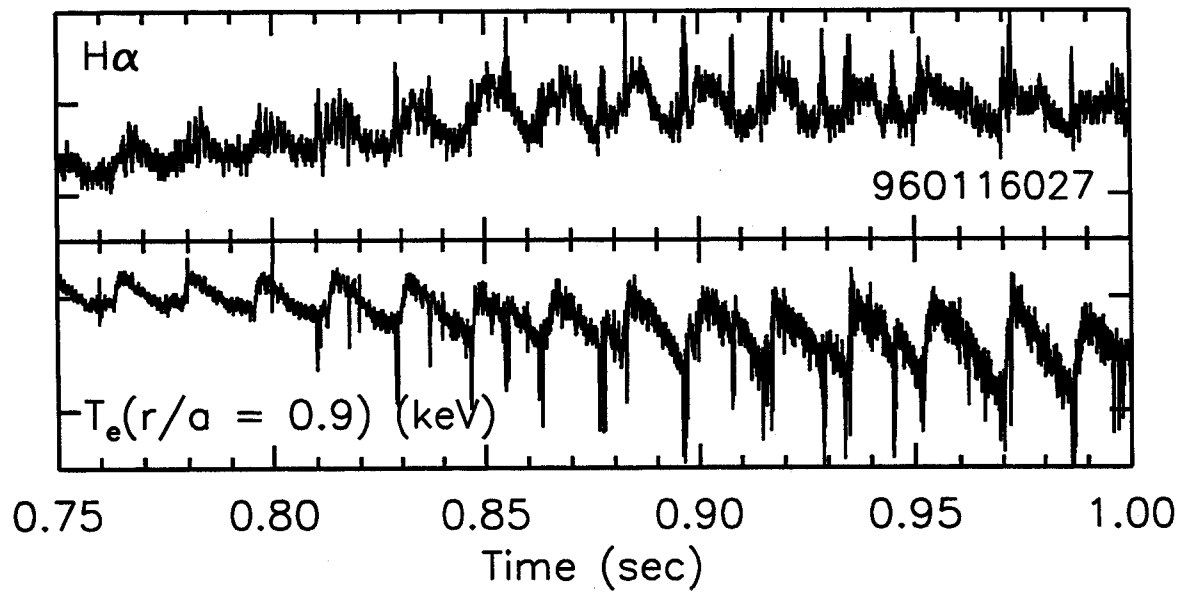


Figure 2(b)



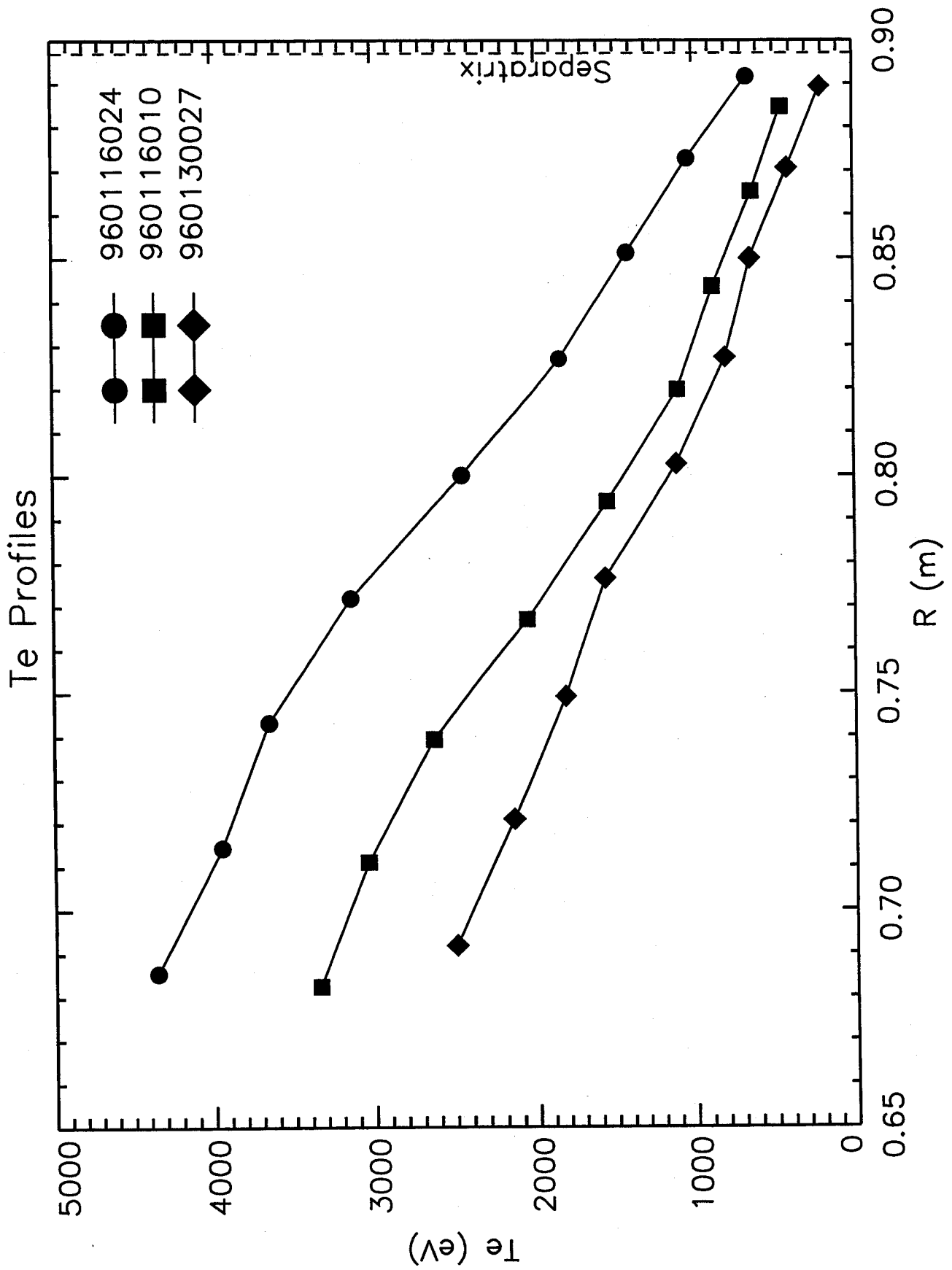


Figure 3

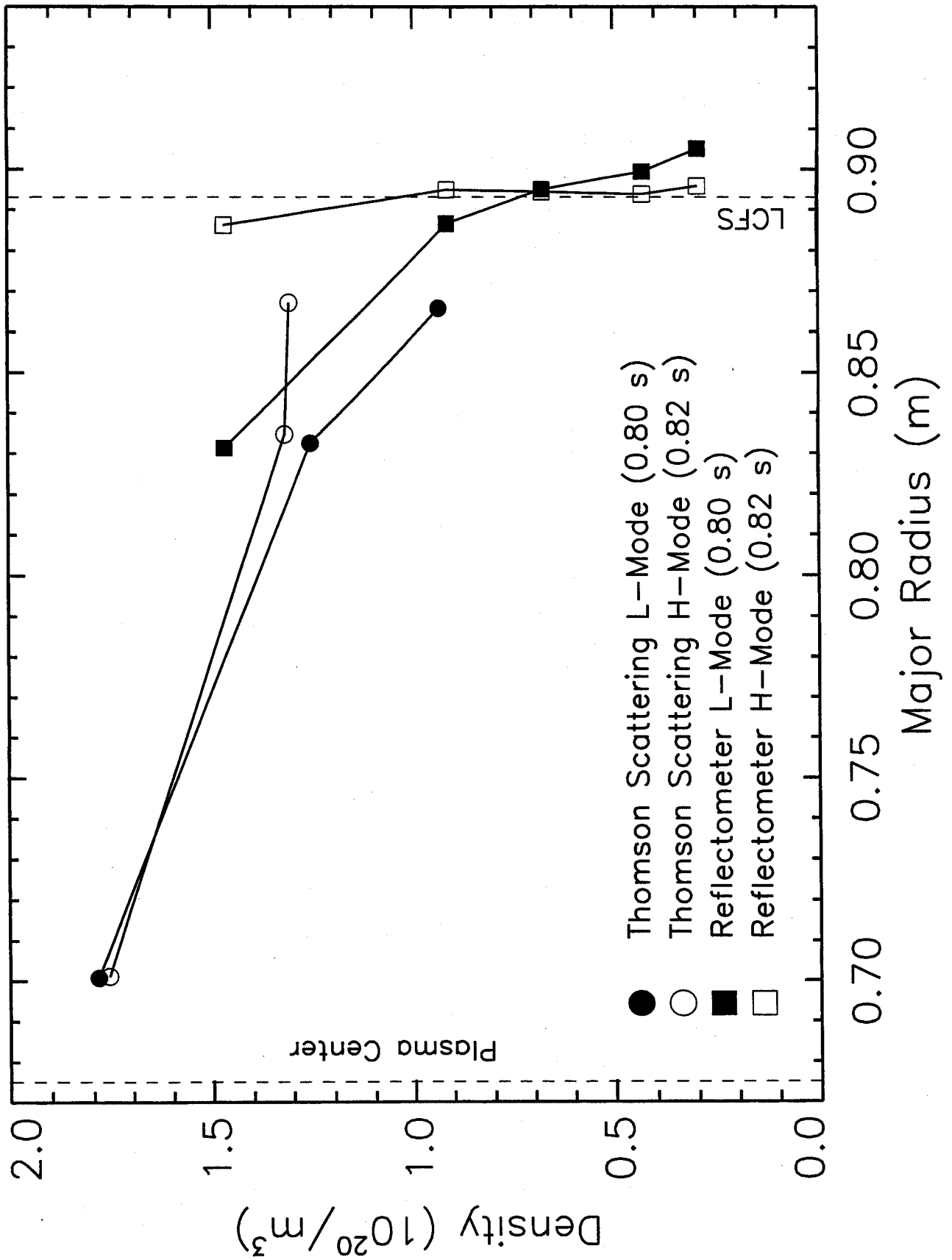


Figure 4

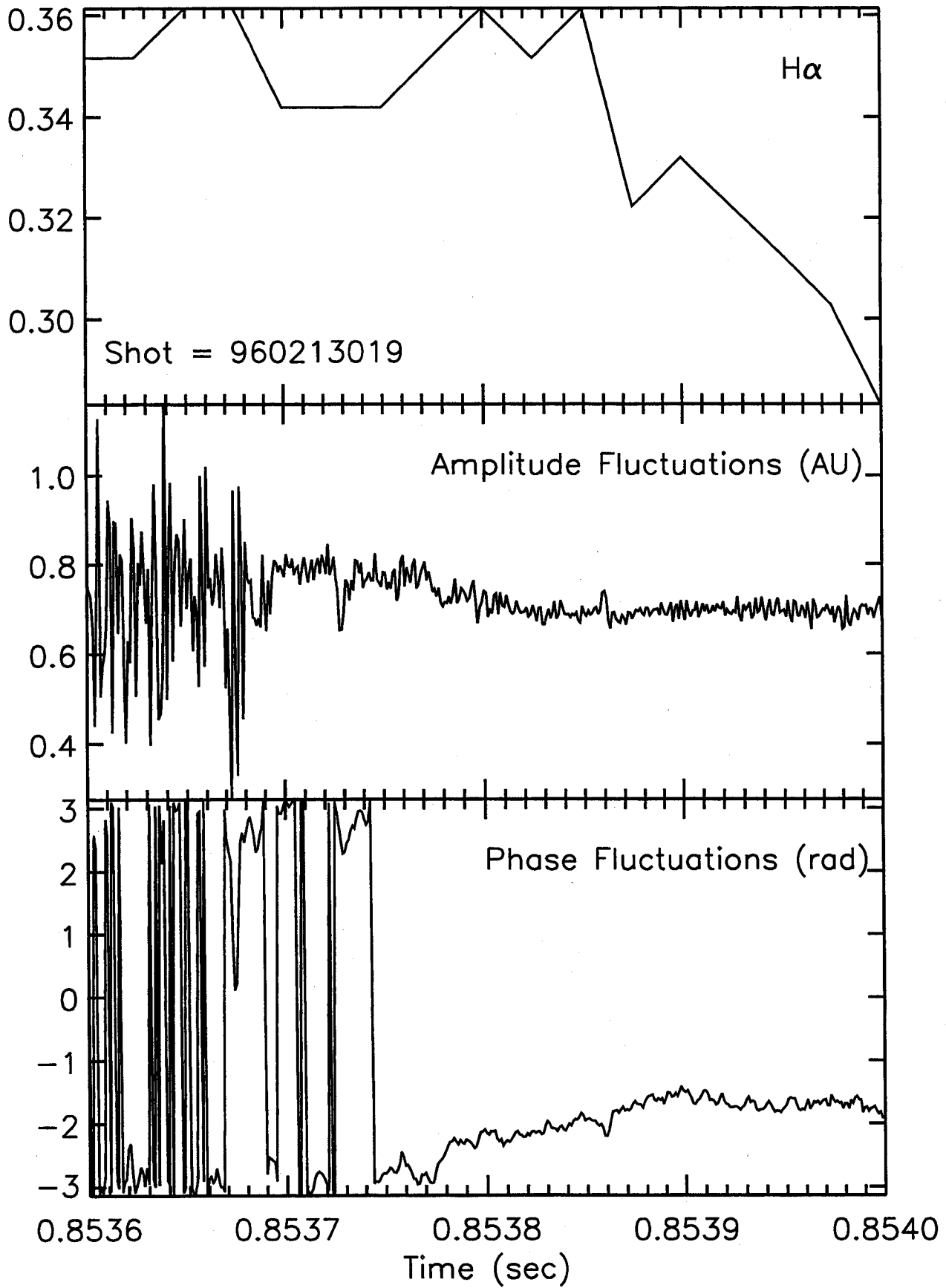


Figure 5

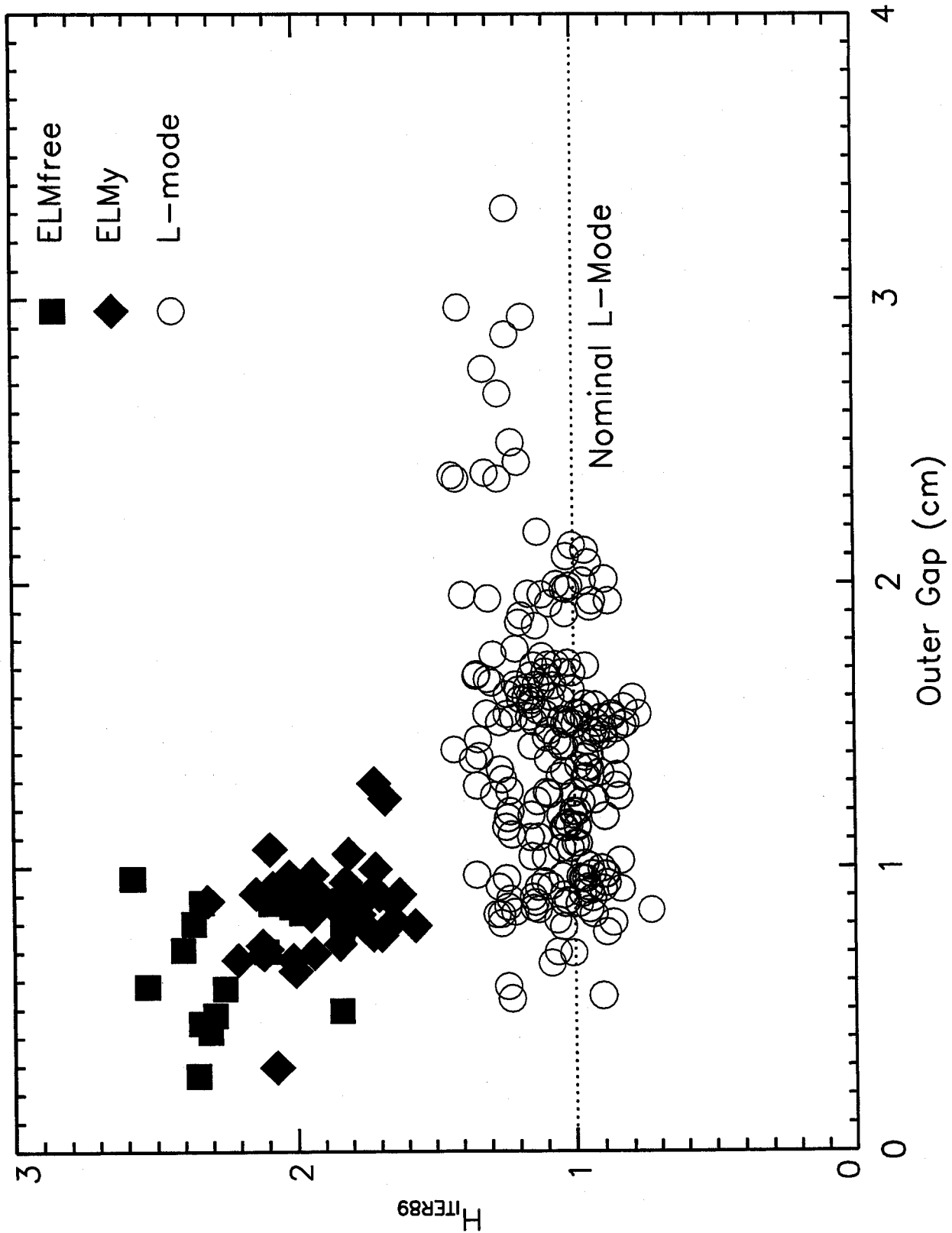


Figure 6

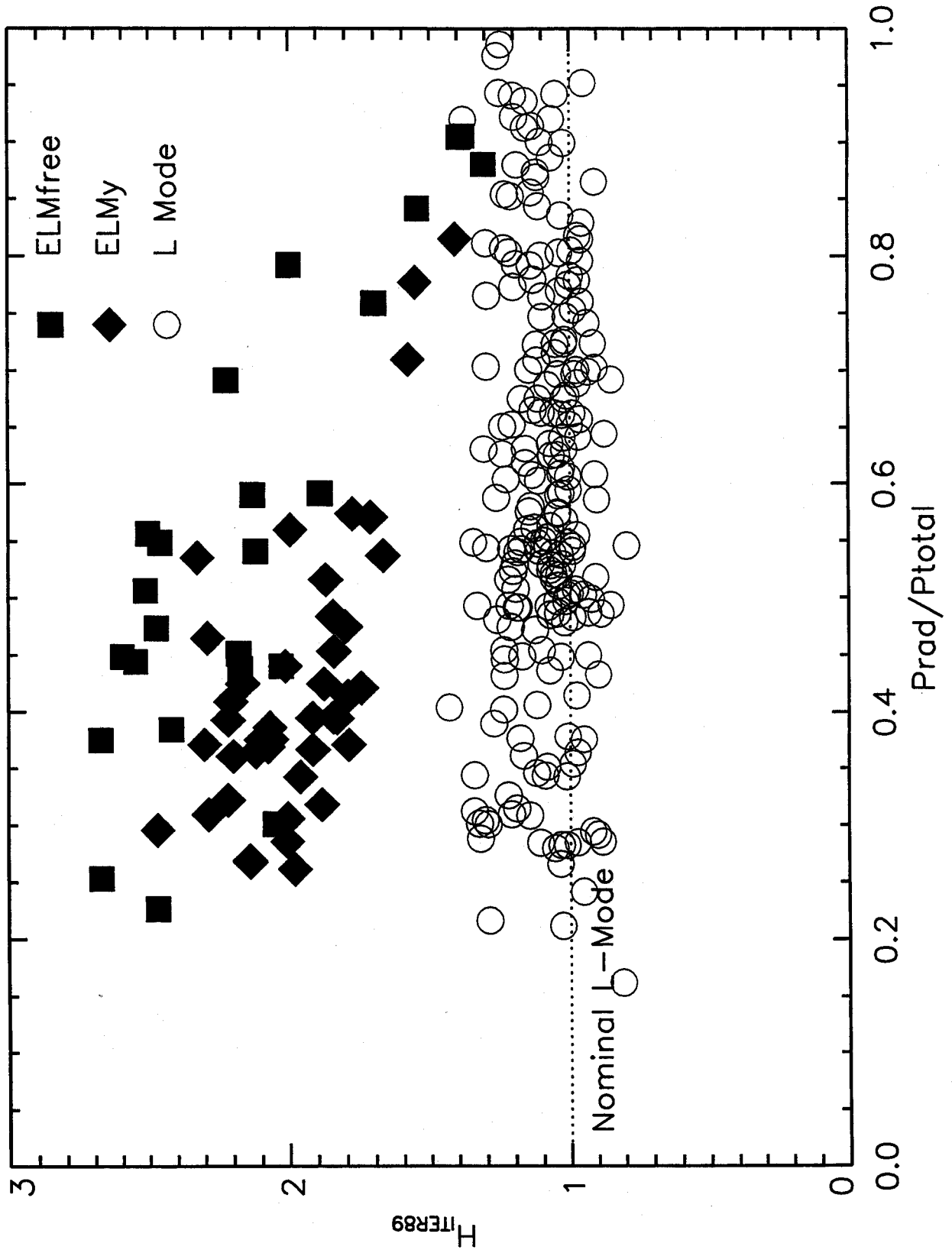


Figure 7

Pre-boronization  
951205026

Post-boronization  
960116010

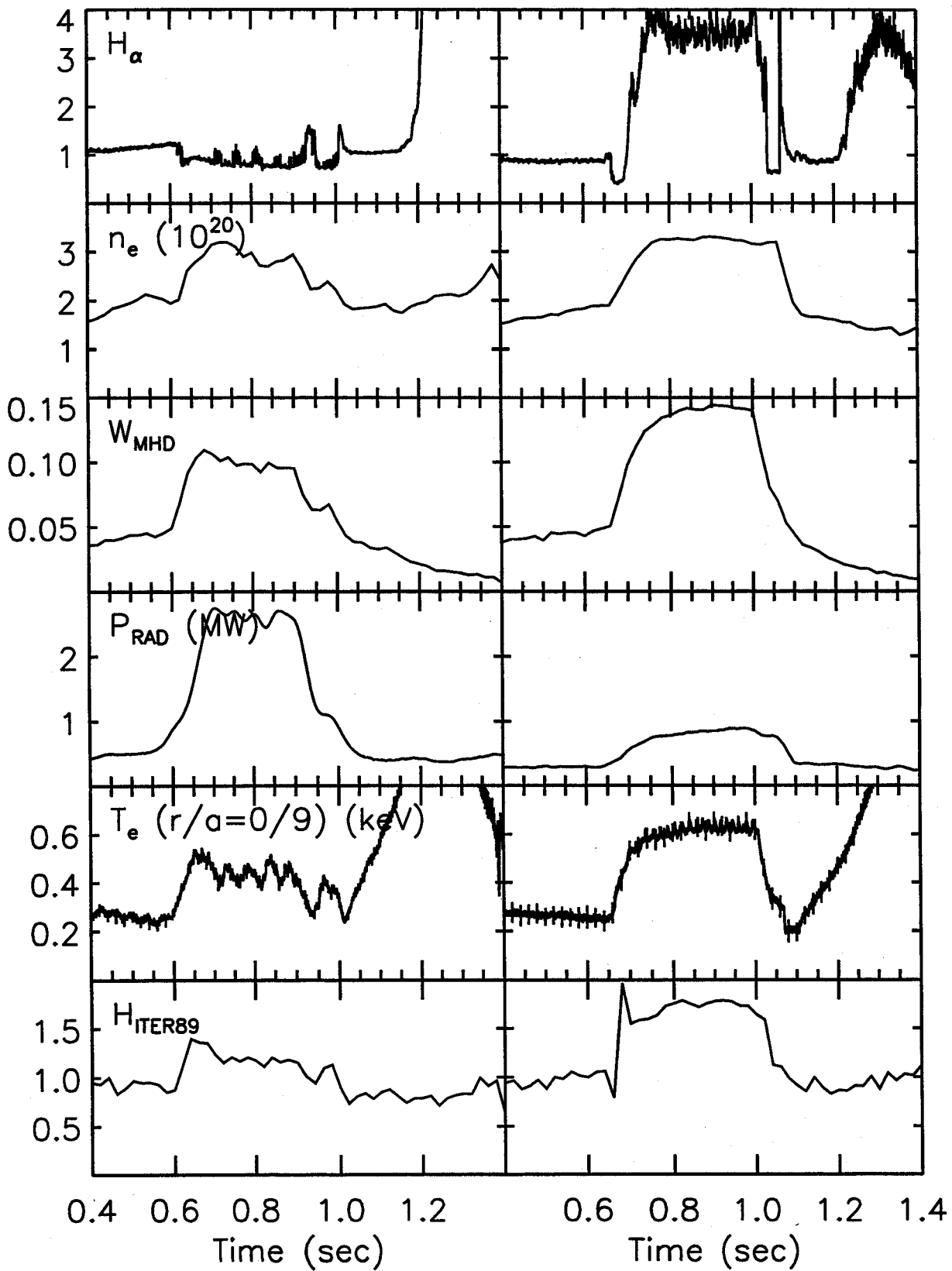


Figure 8

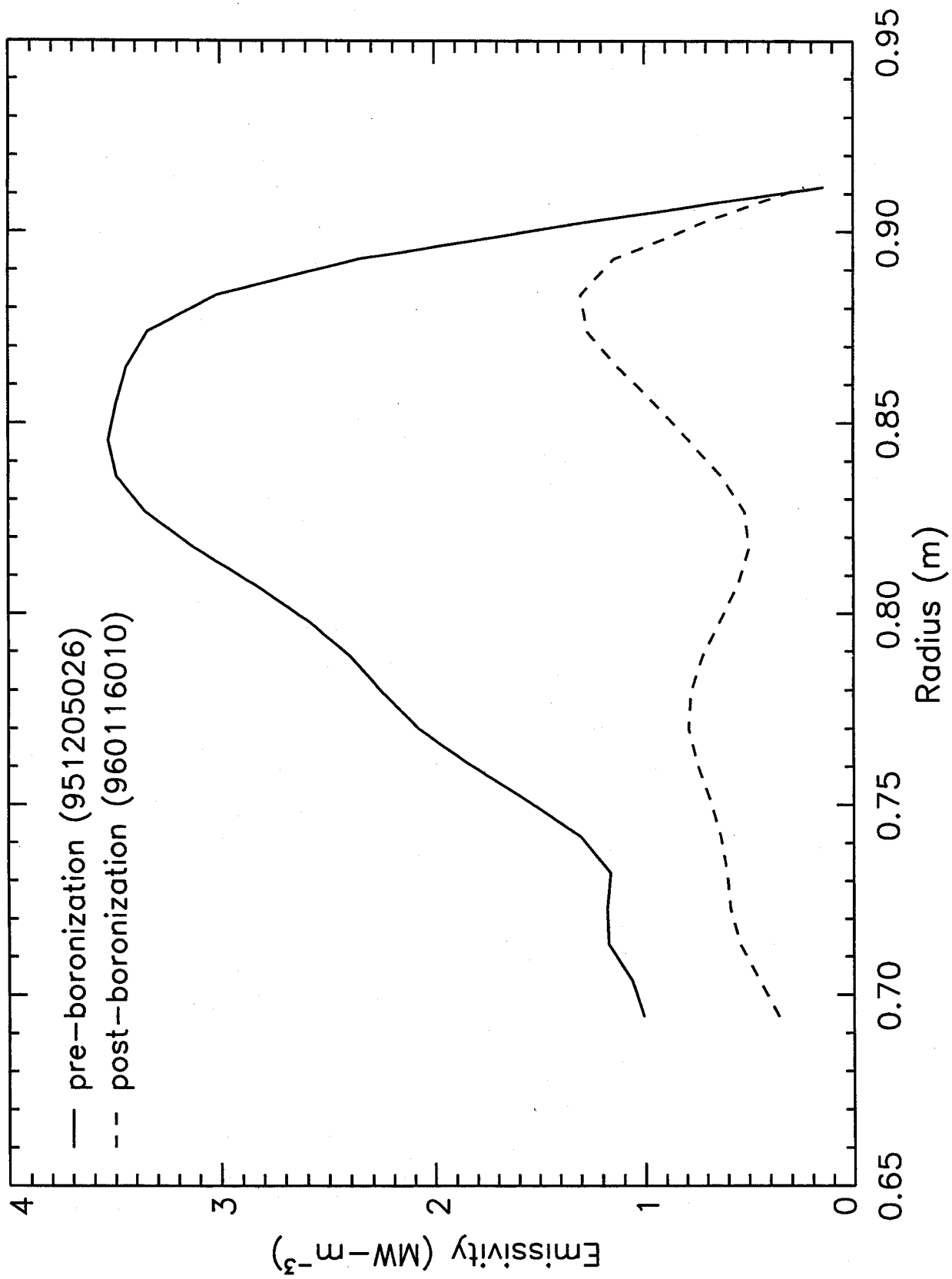


Figure 9

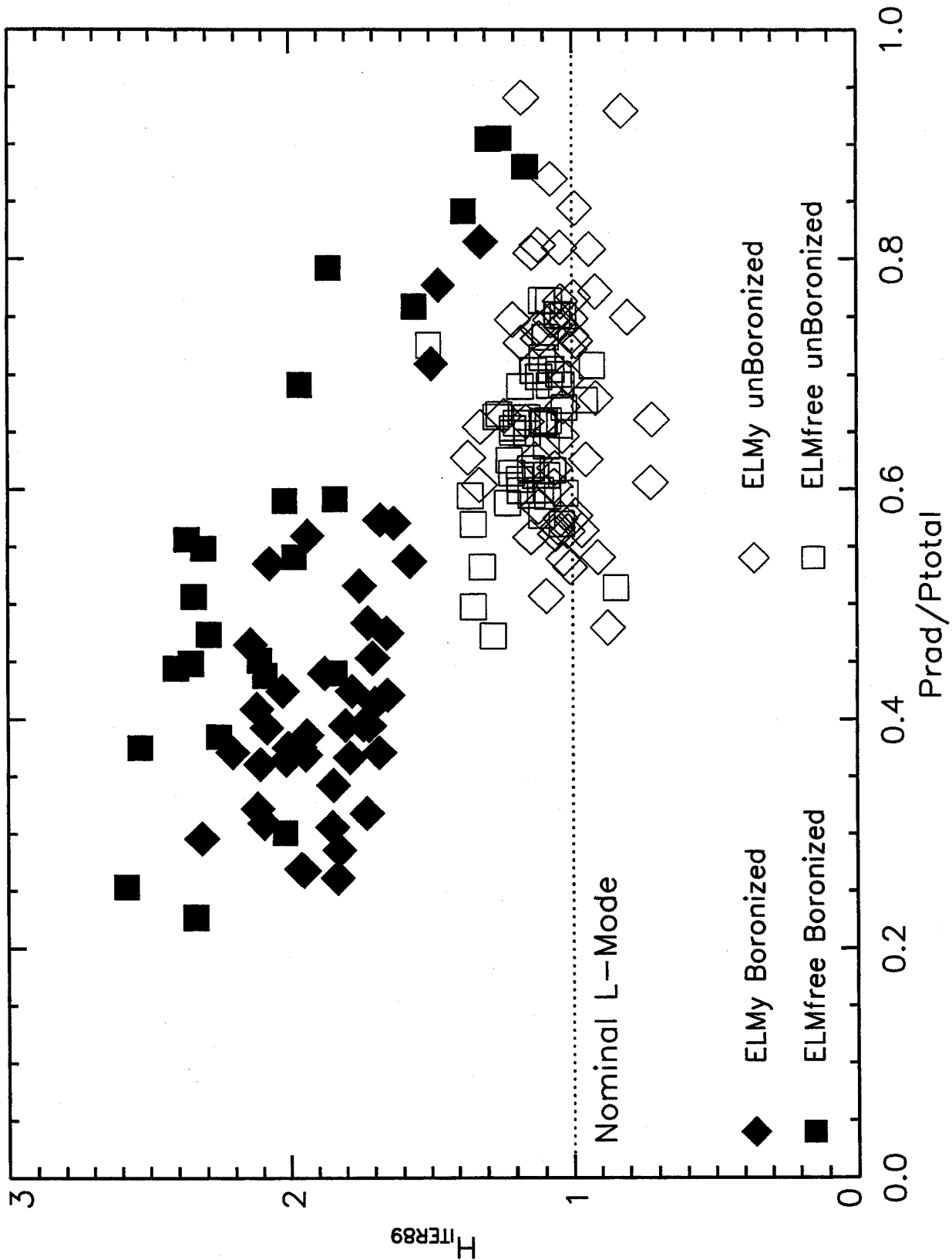


Figure 10



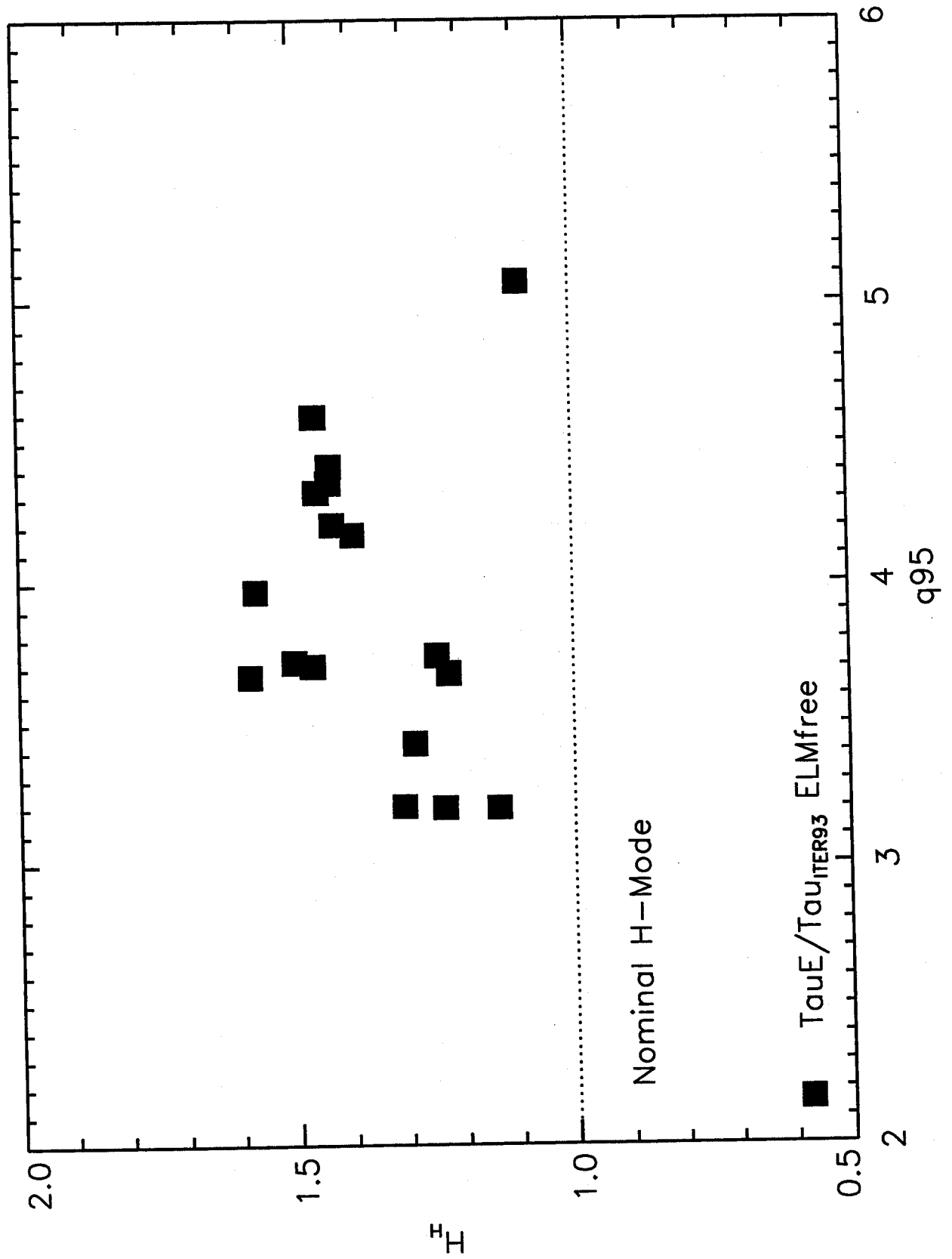


Figure 11

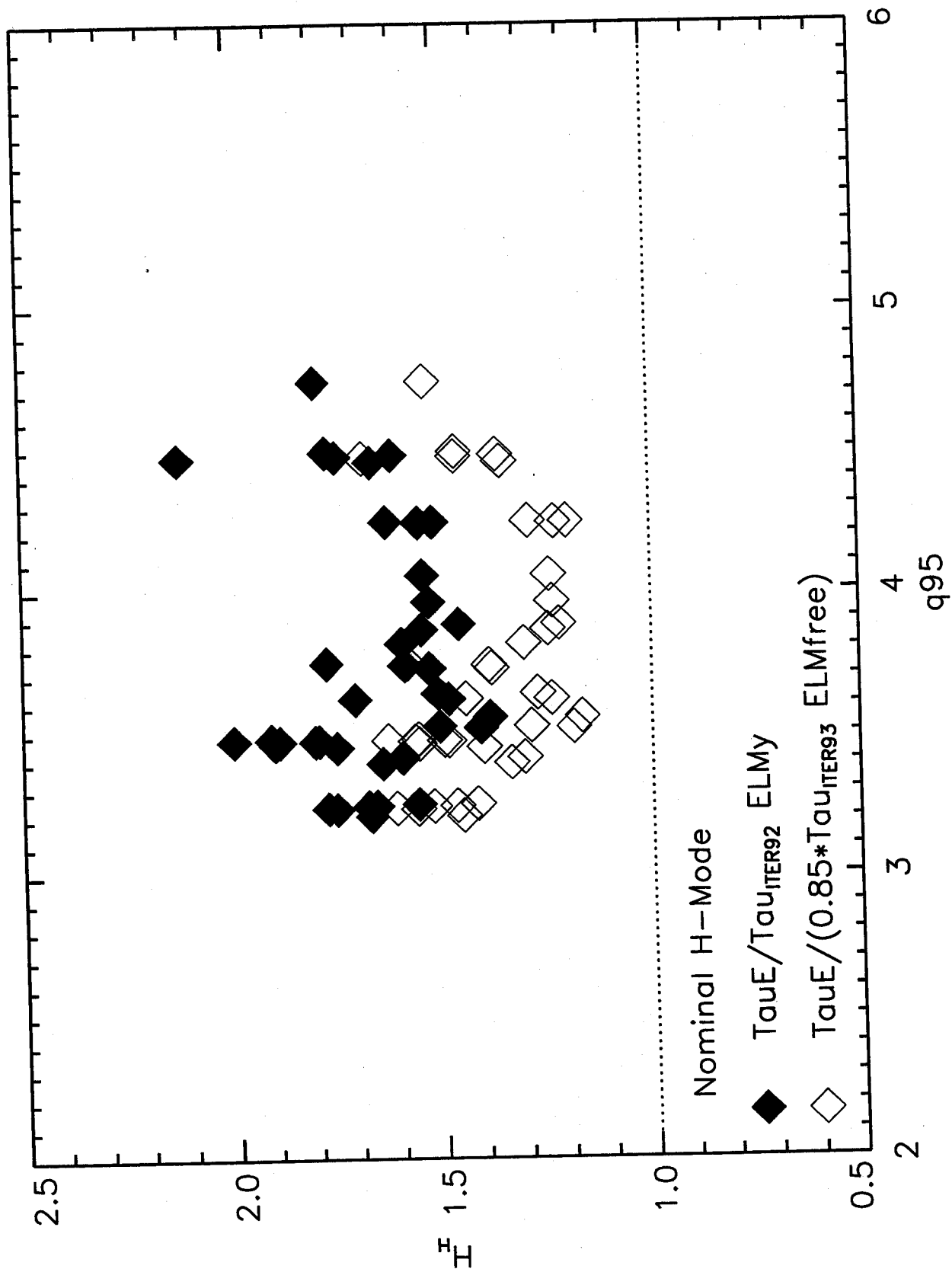


Figure 12

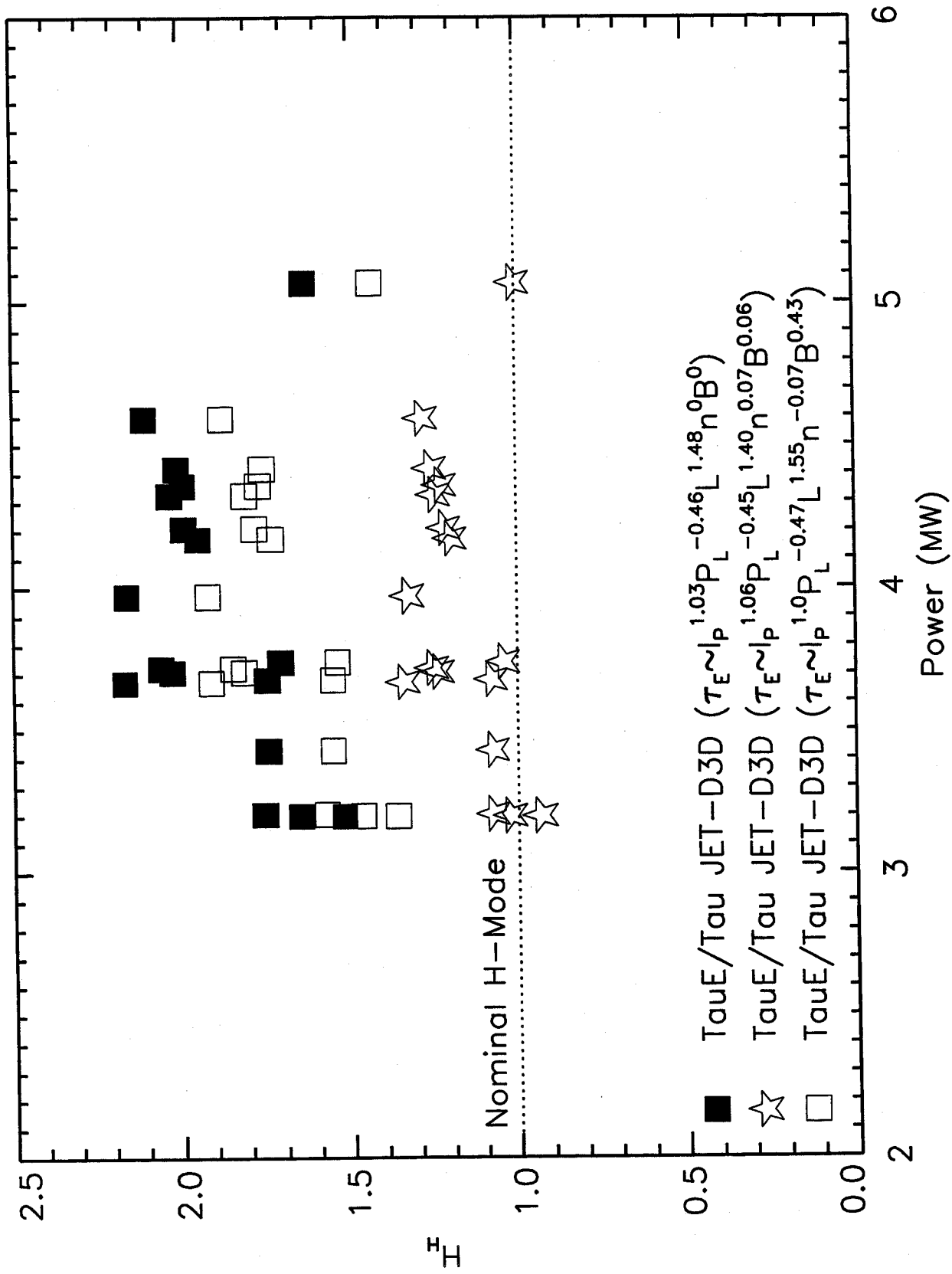


Figure 13

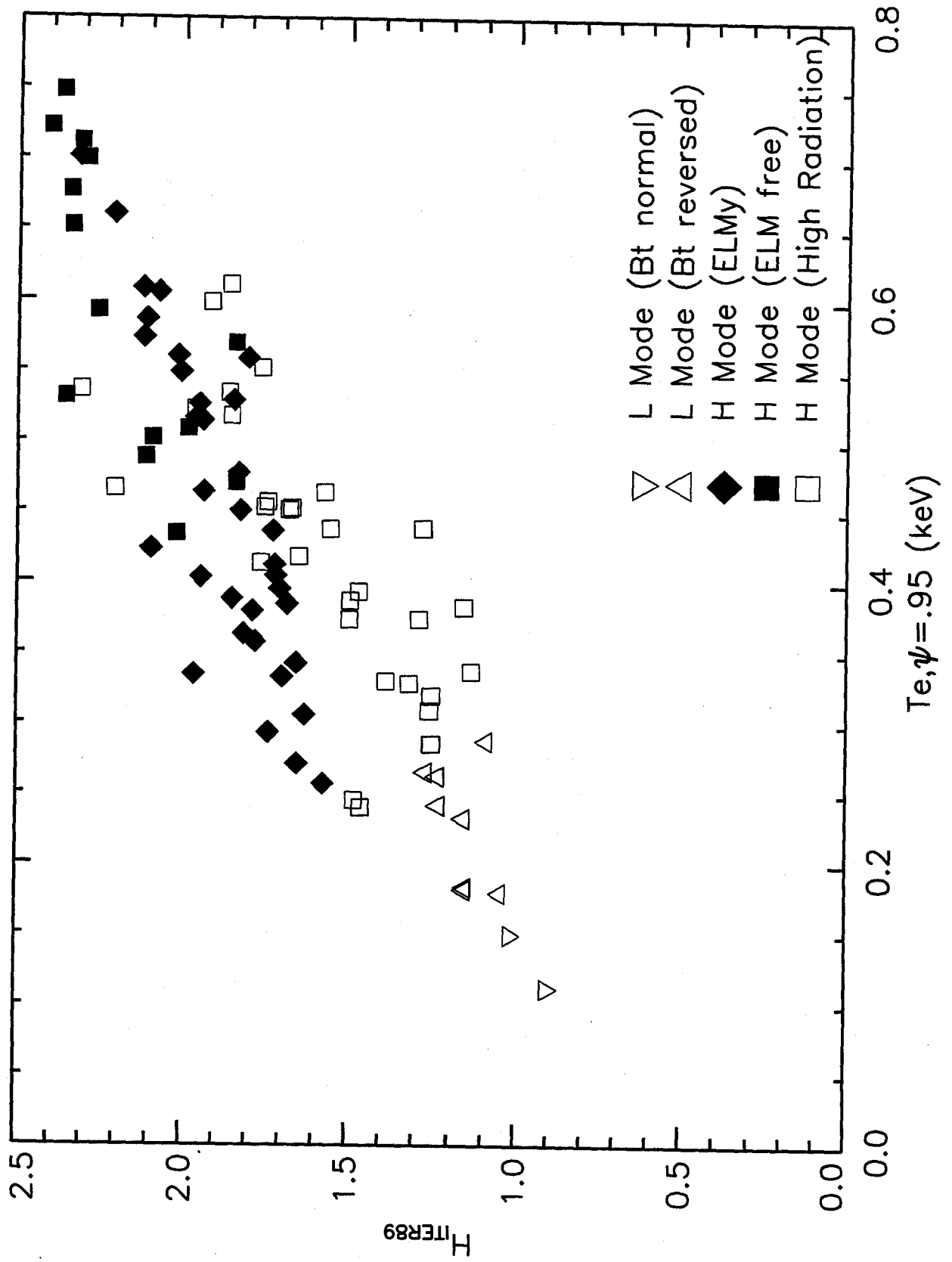


Figure 14

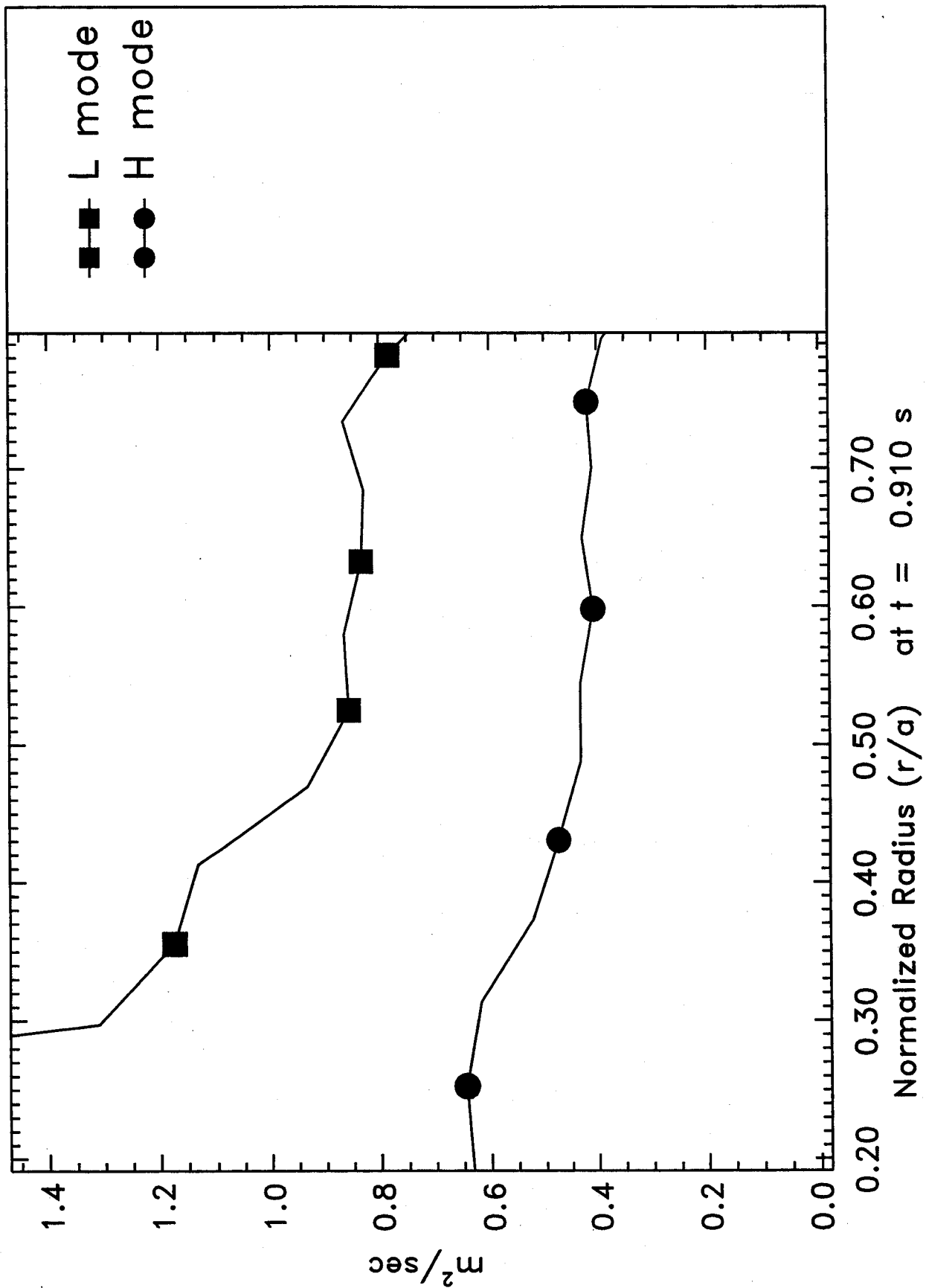


Figure 15

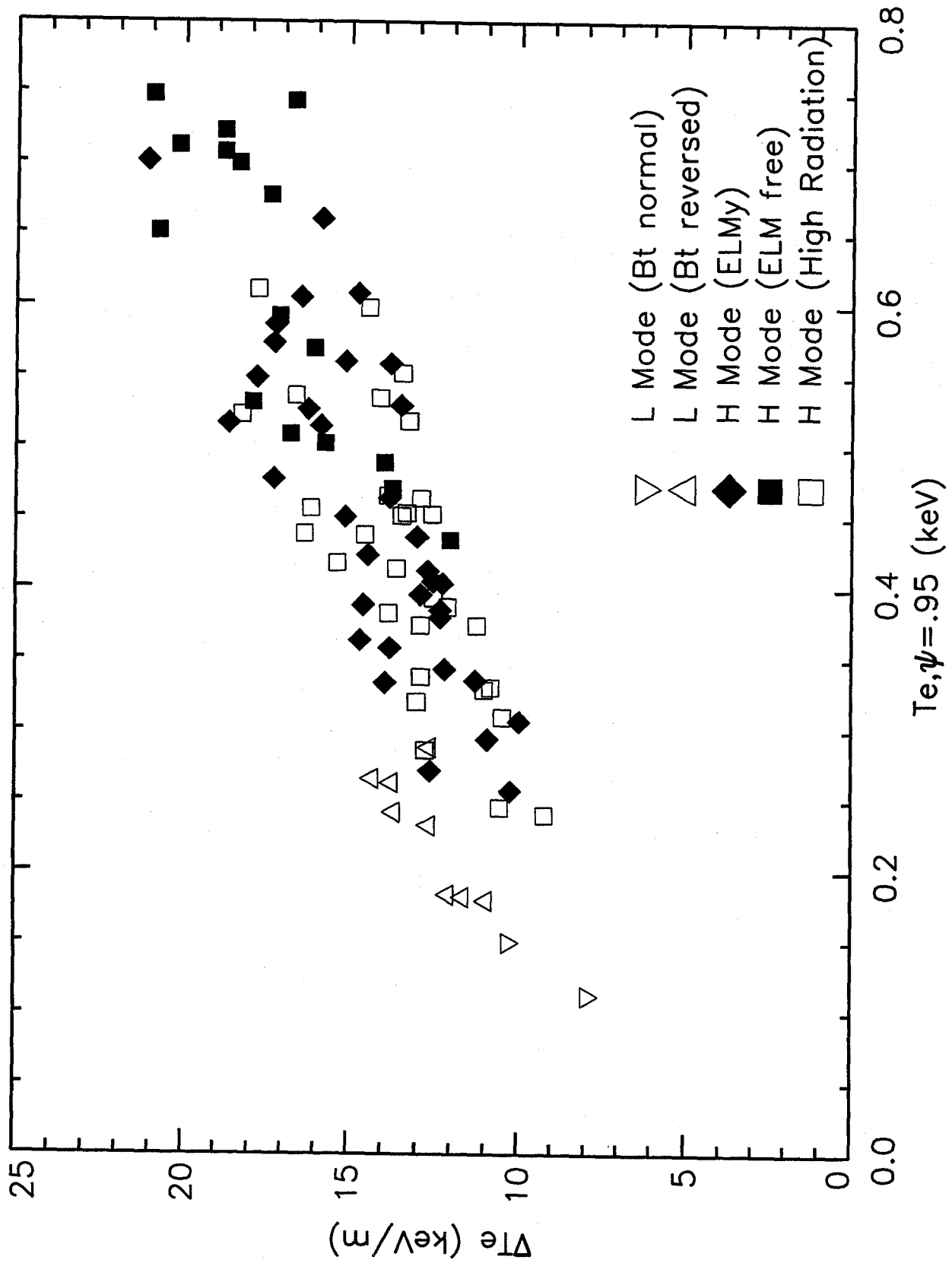


Figure 16

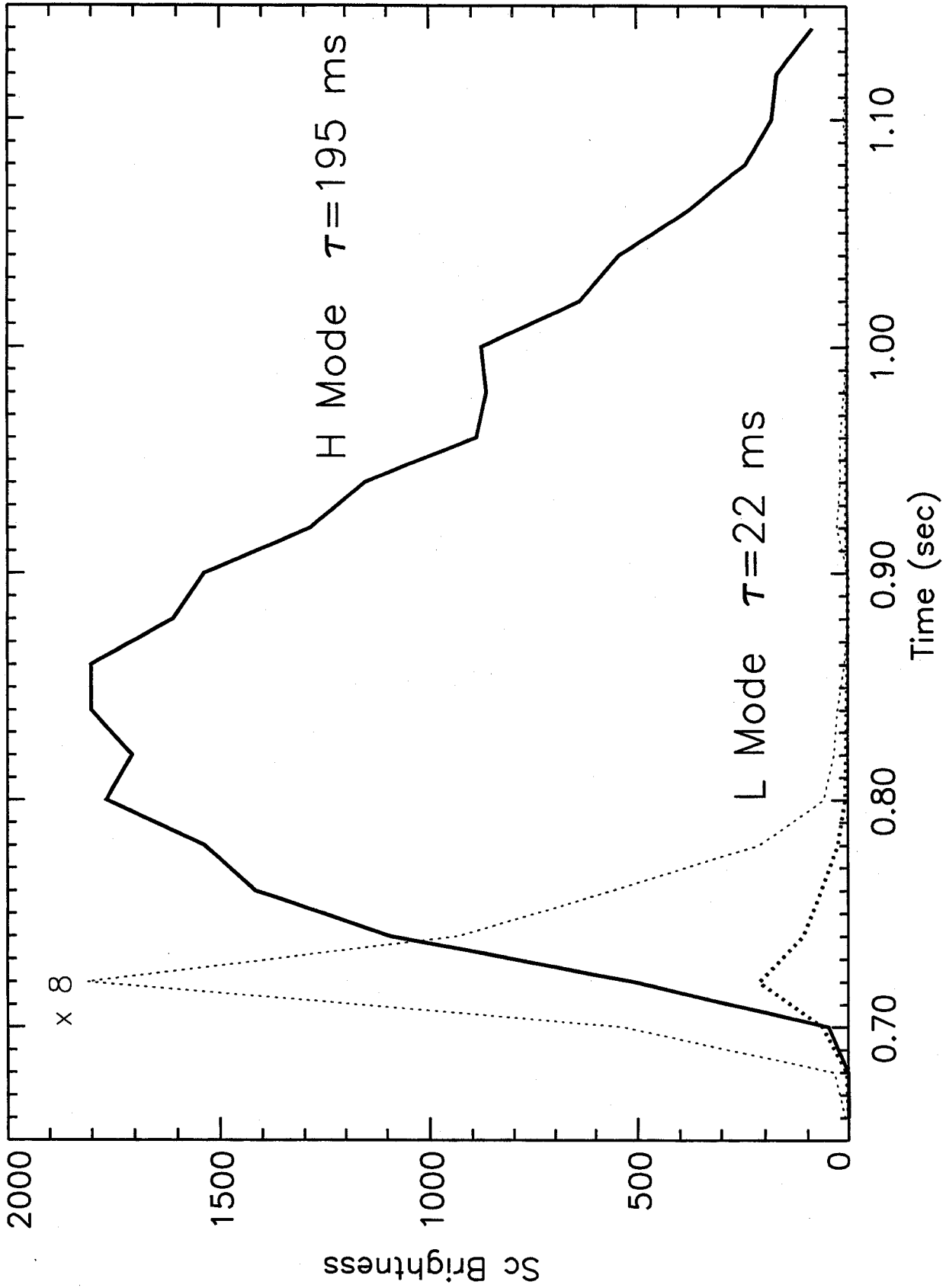


Figure 17

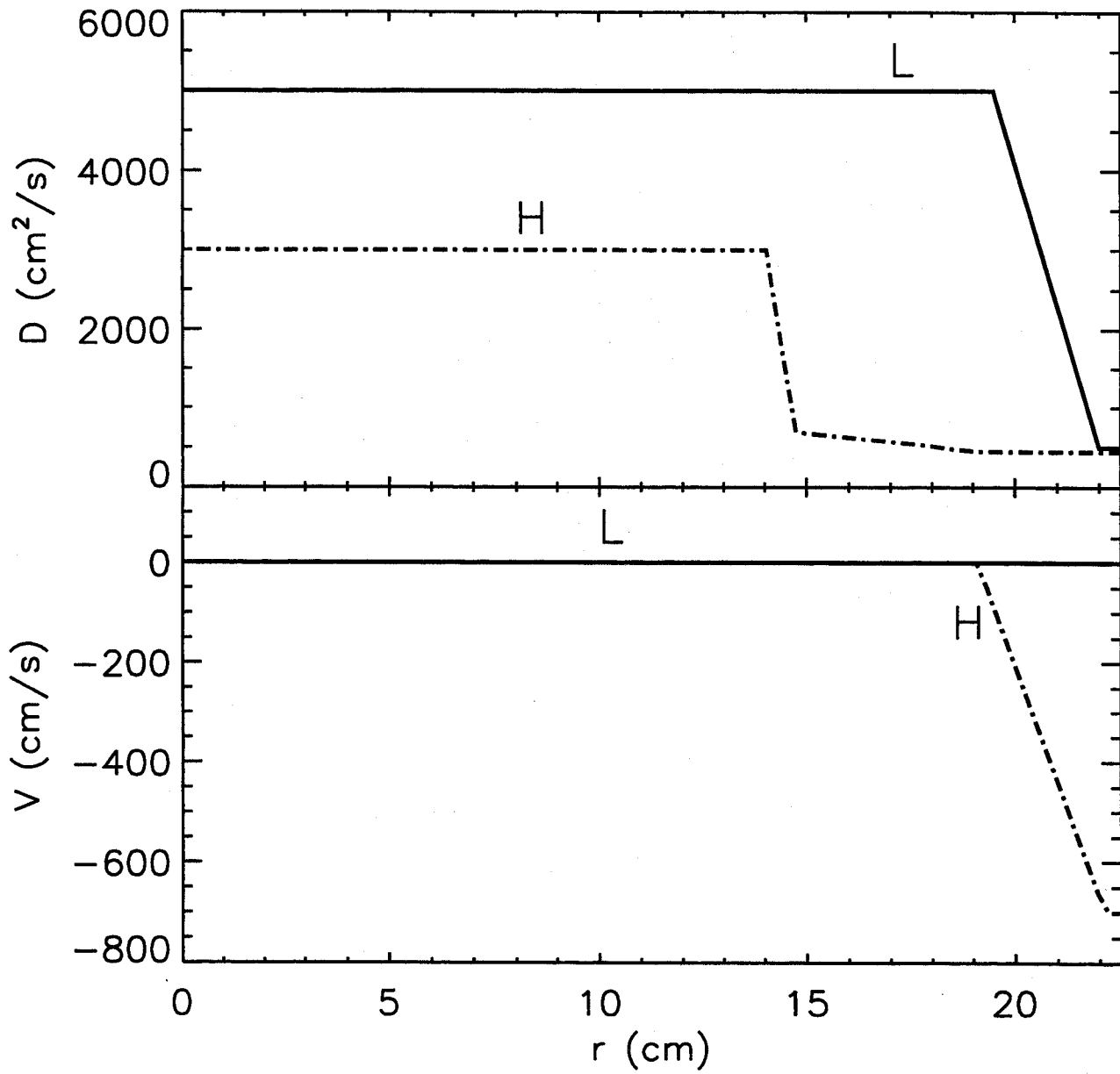


Figure 18